Magnetic induction inspires a schematic theory for crosstalk-driven relaxation dynamics in cells

Kevin R. Pilkiewicz and Michael L. Mayo

Phys. Rev. E **103**, 042417 — Published 20 April 2021

DOI: 10.1103/PhysRevE.103.042417

Magnetic Induction Inspires a Schematic Theory for Crosstalk-driven Relaxation Dynamics in Cells

Kevin R. Pilkiewicz and Michael L. Mayo
U.S. Army Engineer Research and Development Center, Vicksburg MS 39180
(Dated: March 17, 2021)

Establishing formal mathematical analogies between disparate physical systems can be a powerful tool, allowing for the well studied behavior of one system to be directly translated into predictions about the behavior of another that may be harder to probe. In this paper we lay the foundations for such an analogy between the macroscale electrodynamics of simple magnetic circuits and the microscale chemical kinetics of transcriptional regulation in cells. By artificially allowing the inductor coils of the former to elastically expand under the action of their Lorentz pressure, we introduce nonlinearities into the system that we interpret through the lens of our analogy as a schematic model for the impact of crosstalk on the rates of gene expression near steady state. Synthetic plasmids introduced into a cell must compete for a finite pool of metabolic and enzymatic resources against a maelstrom of crisscrossing biological processes, and our theory makes sensible predictions about how this noisy background might impact the expression profiles of synthetic constructs without explicitly modeling the kinetics of numerous interconnected regulatory interactions. We conclude the paper with a discussion of how our theory might be expanded to a broader class of plasmid circuits and how our predictions might be tested experimentally.

I. INTRODUCTION

Just as the functional state of a computer processor is determined by the individual on/off states of its billions of transistors, the biochemical state of a cell is defined by the number of active copies of thousands of different proteins that regulate the cell's basic biological functions and control its response to environmental changes. And just as a computer hacker can install malicious code onto a computer to redirect its processor's functionality towards the surreptitious mining of cryptocurrency, biologists can insert custom DNA "code" in the form of synthetic plasmids into bacterial cells to repurpose their metabolic resources towards the mass production of non-native proteins, among other functions [1, 2]. There is a limit to how much processor power a computer hacker can siphon away before the computer becomes unable to maintain its basic functions and crashes; and there is similarly a metabolic limit [3] to the number of synthetic plasmids that can be inoculated into a bacterial population before the finite metabolic resources of the cells are stretched so thin that they become unable to maintain life-essential functions and die.

The mutual reliance of cellular processes on a shared and limited pool of biochemical resources is one form of biological *crosstalk* [4, 5]. Because this crosstalk formally interconnects all of the numerous regulatory processes controlling the cell's internal state, its impact on any particular process or set of processes can be difficult to model. Even an especially simple bacterium like *Escherichia coli* has over three thousand processes in its transcriptional network alone [6], and proteins like RNA polymerase–the principal enzyme responsible for the transcription of a gene into a strand of mRNA–must be shared across all of them. This complexity is problematic, because synthetic biologists often want a way to predict *a priori* how efficiently a recombinant plasmid will execute its function inside a bacterial population and to what extent the overall growth and resilience of the population will be impacted in return. The traditional modeling approach used to address these concerns is the flux-balance model, in which a large set of rate laws governing the usage, production, and uptake of metabolic resources by various cellular processes are taken into account and simultaneously solved numerically [7]. Modern computational resources have enabled some of these models to exhaustively account for most or all relevant processes (genome-scale models) [8], whereas older iterations were forced to rely upon a coarse-grained approach that empirically modeled the fluxes of a limited number of key resource pools, such as amino acids, nucleotides, etc [9, 10].

Chemical kinetics has also been employed to model the effects of shared cellular resources [11, 12], typically by using a more granular model of gene transcription that accounts for limited concentrations of RNA polymerase, ribosomes, and DNA binding sites. Both kinetics and flux-balance modeling paradigms have typically focused on making estimates of steady-state gene expression levels or cellular growth rates, but synthetic biology has increasingly focused on developing plasmid circuits with dynamic expression signatures, such as oscillators [13–15], which express a desired gene in periodic pulses, or logic gates [16–18], which get expressed only under specific conditions. To understand how crosstalk impacts the responsiveness or reliability of these more sophisticated circuits, a good starting point is to characterize how it changes their dynamic response to small fluctuations that push the cell away from homeostasis. Even with the simplifications of existing models, robustly characterizing this response would still require probing the topology of a rather high-dimensional dynamical manifold. It would be ideal if the impact of crosstalk on the proteins of interest could be treated in a manner that

did not require modeling fluctuations in a large number of extraneous chemical species.

Physics is replete with examples of disparate physical processes that can be characterized by structurally similar mathematical models. The assumption that a rate of flow is driven by a linear dependence on a spatial gradient, for example, results in Fourier's law of heat transfer, Ohm's law of current flow, Fick's law of diffusion, and Poiseuille's law of fluid flow. Similarly, the Ising spin model can be used analogously to model the alignment of magnetic domains in a ferromagnet, the thermodynamic states of a binary alloy, or the dynamics of a lattice gas. Inspired by these examples, we attempt to characterize a much simpler, schematic description of the dynamic response to cellular crosstalk by first pursuing a mathematical formalization of the vague analogy often made between plasmid circuits and their electronic counterparts.

Both electronic and genetic circuits involve closed loops of specialized, interacting components, but making any sort of generalized comparison has proven to be elusive [19–21]. We make progress in resolving this difficulty by drawing an analogy between chemical concentrations and electric currents. In chemical kinetics, the time rate of change in one chemical population is a function of the concentrations of one or more others; in magnetic induction, an inverted mathematical structure holds wherein the strength of an induced electric current is a function of the time rates of change of one or more other currents. We demonstrate that, so long as we restrict our attention to a linear regime and satisfy a couple additional caveats, there is a one-to-one mapping between the differential equations governing these two phenomena that enables us to directly relate the linear response of protein concentrations near steady state to the dynamic loop currents of a certain class of magnetic circuits.

Competition for resources in gene circuits has previously been modeled analogously to multiple resistors in series [22, 23], but this formalism does not avoid the problem of needing to know the dynamic concentrations of a potentially prohibitive number of chemical species in order to describe the response of a protein of interest to a fluctuation in its concentration. We attempt to sidestep this issue within our magnetic analogy by allowing for inductor coils that elastically expand under their own Lorentz pressure. This construction, though physically unrealistic in the electronics context, results in current relaxation profiles that match our experimentally-informed intuition [24] for how limited cellular resources should impact the relaxation kinetics of a protein near steady state. In two specific cases, we then show how to qualitatively reproduce the resultant nonlinear current dynamics with the kinetics of a sequence of elementary chemical reactions, and we discuss how those reactions can be meaningfully interepreted as schematic models of cellular crosstalk that involve only a small number of "virtual" chemical species. While these simplified kinetic models succeed in capturing the phenomonology of crosstalk, it remains to be seen to what extent this framework can be leveraged to make novel predictions about the dynamical behavior of real biological circuits of interest; so, with that in mind, we conclude by discussing how some of our more restrictive assumptions might be relaxed to extend our analogy to more complex dynamical circuits, and we summarize the sort of experiments that would be required to validate the predictive power of our models.

II. METHODS

The basic analogy that we propose can be derived in general terms rather straightforwardly. Let $\{[X_i]_t\}$ be a set of relevant, time-dependent biomolecular concentrations, indexed $1, \ldots, N$, that are related to one another by the following set of coupled differential equations:

$$\frac{d[X_i]_t}{dt} = f_i(\{[X_i]_t\}), \tag{1}$$

where each $f_i(\{[X_i]_t\})$ is some generally nonlinear function of the various concentrations in the set. For dynamics consisting of sufficiently small fluctuations near steady state, we can linearize Eq. (1) into a matrix equation of the following form:

$$\frac{d}{dt}\delta[\mathbf{X}]_t = \mathcal{K}\delta[\mathbf{X}]_t, \tag{2}$$

where the i^{th} component of the vector $\delta[\mathbf{X}]_t$ is the deviation of concentration $[X_i]_t$ from its steady-state average and $\mathcal{K}$ is a matrix of linearized kinetic rate constants.

For a set of independent loop currents coupled to each other only through magnetic induction, we can write a similar matrix equation, assuming we restrict our attention to linear circuits:

$$\delta\mathbf{I}(t) = \mathcal{L}\frac{d}{dt}\delta\mathbf{I}(t). \tag{3}$$

In the above, $\delta\mathbf{I}(t)$ is now the vector of current fluctuations from steady state, and $\mathcal{L}$ is the matrix whose diagonal elements are proportional to the linear inductances L_i and whose off-diagonal elements are proportional to the mutual inductances M_{ij}. So long as $\det\mathcal{L} \neq 0$, this matrix will be invertible, and we can express Eq. (3) in a form analogous to that of Eq. (2):

$$\frac{d}{dt}\delta\mathbf{I}(t) = \mathcal{L}^{-1}\delta\mathbf{I}(t), \tag{4}$$

and we can map one set of equations to the other by identifying $\delta[X_i]_t = \delta I_i(t)$ and requiring that $\mathcal{K}_{ij} = \mathcal{L}^{-1}_{ij}$ for all $i, j = 1, \ldots, N$.

In the subsections that follow, we apply this formalism to two simple plasmid circuits and their proposed magnetic analogues, explicitly deriving the parameter mappings necessary for equivalence in each case. We then proceed to introduce our conception of what we term an

"elastic" inductor and discuss how its nonlinear behavior is representative of a kind of magnetic crosstalk that is phenomenologically similar to what we expect to see from genetic crosstalk in cells.

A. The Simplest Plasmid Circuit

The first gene circuit we consider consists of a plasmid ring containing only a single gene encoding some protein X and a promoter site. We assume that X is regulated constitutively at a constant rate k_X and degraded at a rate proportional to its concentration $[X]$. The time-dependent concentration $[X]_t$ consequently obeys the following linear, ordinary differential equation:

$$\frac{d[X]_t}{dt} = k_X - k_D[X]_t, \tag{5}$$

where k_D is the degradation frequency. Recognizing that the steady-state concentration $\langle[X]\rangle$ must equal k_X/k_D, we can recast this equation in terms of the concentration fluctuation $\delta[X]_t \equiv [X]_t - \langle[X]\rangle$:

$$\frac{d\delta[X]_t}{dt} = -k_D\delta[X]_t. \tag{6}$$

Given an initial fluctuation away from steady state, $\delta[X]_0$, this equation is trivial to solve, yielding a simple exponential decay back towards steady state over a characteristic time scale $1/k_D$:

$$\delta[X]_t = \delta[X]_0 e^{-k_D t}. \tag{7}$$

We now proceed to demonstrate that the above kinetics are completely analogous to the current dynamics of a simple RL-circuit consisting of a voltage source V, a resistor with resistance R, and an inductor with inductance L connected in series. According to Kirchhoff's Voltage Law, the total voltage V must equal the sum of the voltage drops across the resistor and the inductor, leading to the following equation:

$$V = RI(t) + L\frac{dI(t)}{dt}, \tag{8}$$

where $I(t)$ is the dynamic current of the circuit loop. The above can be immediately manipulated into the form of Eq. (6) by defining $\delta I(t) \equiv I(t) - V/R$:

$$\frac{d\delta I(t)}{dt} = -\frac{R}{L}\delta I(t), \tag{9}$$

and an equivalence can be established by setting $\delta I(t) = \delta[X]_t$ and $R/L = k_D$. See Fig. 1 for a pictorial comparison of these two circuit analogues.

B. A Mutually Regulating Plasmid Circuit

The next plasmid we consider consists of two genes that encode proteins called X and Y, along with their corresponding promoter sites. We assume that protein X can bind to the promoter site of the Y gene to regulate its transcription, and we likewise assume that protein Y can regulate protein X in a similar fashion. Assuming that proteins X and Y have respective basal transcription rates k_X and k_Y and respective degradation frequencies k_D and k'_D, their concentrations should each obey a pair of coupled differential equations with the following general form:

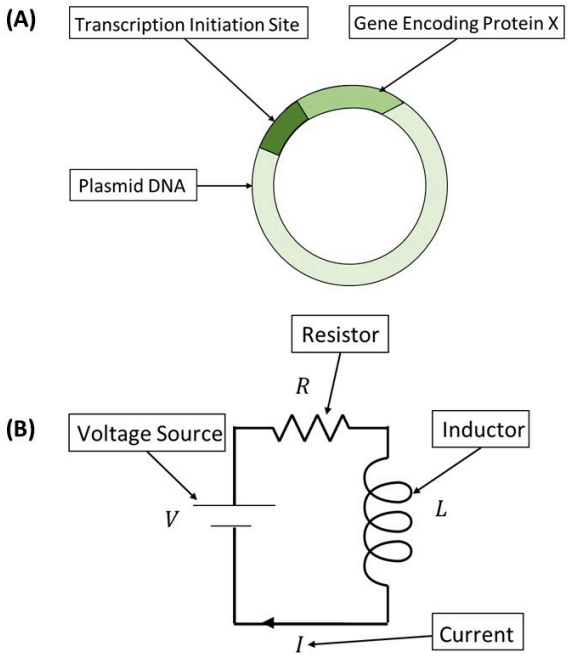

FIG. 1. Analogous circuits. (A) A schematic representation of a simple plasmid circuit consisting of a single, constitutively regulated gene and (B) a schematic diagram of its equivalent magnetic circuit, drawn using standard linear circuit notation for its various components.

$$\begin{aligned}\frac{d[X]_t}{dt} &= G_{XY}([Y]_t) + k_X - k_D[X]_t \\ \frac{d[Y]_t}{dt} &= G_{YX}([X]_t) + k_Y - k'_D[Y]_t.\end{aligned} \tag{10}$$

In the above, $G_{XY}([Y])$ and $G_{YX}([X])$ are general functions representing the typically nonlinear binding kinetics of the transcription factors X and Y to their respective promoter sites. Oftentimes, these functions are well approximated as Hill functions [25], but we will only be concerned with the dynamics of this system near steady state, in which case we can linearize the kinetics of Eq. (10) to obtain the following matrix equation:

$$\frac{d}{dt}\begin{pmatrix}\delta[X]_t \\ \delta[Y]_t\end{pmatrix} = \begin{pmatrix}-k_D & \pm k_{XY} \\ \pm k_{YX} & -k'_D\end{pmatrix}\begin{pmatrix}\delta[X]_t \\ \delta[Y]_t\end{pmatrix}. \tag{11}$$

The linearized rate constant for the transcriptional regulation of protein X by protein Y is $k_{XY} \equiv |G'_{XY}(\langle[Y]\rangle)|$, i.e., the absolute value of the derivative of the function

G_{XY} evaluated at $\langle[Y]\rangle$. The other linearized rate constant, k_{YX}, is defined analogously. For each of these rate constants, the plus sign is chosen in Eq. (11) if the regulation is promoting, and the negative sign is chosen if it is inhibiting.

For simplicity, we have assumed that this chemical system has only a single, stable fixed fixed point, about which the concentrations of X and Y will fluctuate during homeostasis, and this imposes restrictions on the parameters of the model. First, the steady state is defined by the following pair of equations:

$$\begin{aligned}\langle[X]\rangle &= \frac{1}{k_D}\left[G_{XY}(\langle[Y]\rangle) + k_X\right] \\ \langle[Y]\rangle &= \frac{1}{k'_D}\left[G_{YX}(\langle[X]\rangle) + k_Y\right],\end{aligned} \tag{12}$$

which, by assumption, must have a unique, nontrivial solution. Furthermore, in the case where both transcriptional regulations are either promoting or inhibiting, the condition $k_D k'_D > k_{XY}k_{YX}$ must hold; otherwise, the fixed point at steady state will become unstable, and any small fluctuation will rapidly grow without bound. There are of course some two-component kinetic systems whose nonlinearities give rise to multiple stable fixed points [26], and we shall discuss briefly in the conclusions section how our analogy might be extended to consider a more complex case like this.

In order to have a consistent analogy, the magnetic analogue circuit corresponding to this mutually regulating plasmid must decouple into a pair of independent RL-circuit loops, like that shown in Fig. 1(B). The coupling between these two circuits will be achieved by connecting their inductors with a loop of ferromagnetic material, resulting in a simple transformer circuit. A diagram of this circuit can be found alongside a schematic of its plasmid analogue in Fig. 2. Once again invoking Kirchhoff's Voltage Law, we can express the coupled current dynamics of this circuit by the following pair of equations:

$$\begin{aligned}V_1 &= R_1 I_1(t) + L_1\frac{dI_1(t)}{dt} \pm M\frac{dI_2(t)}{dt} \\ V_2 &= R_2 I_2(t) + L_2\frac{dI_2(t)}{dt} \pm M\frac{dI_1(t)}{dt},\end{aligned} \tag{13}$$

where indices 1 and 2 differentiate the components of the two RL-circuits and M is the mutual inductance between them. Noting once more that $\langle I_i\rangle = V_i/R_i$, these differential equations can be rewritten in the matrix form of Eq. (3):

$$\begin{pmatrix}\delta I_1(t) \\ \delta I_2(t)\end{pmatrix} = \begin{pmatrix}-L_1/R_1 & \mp M/R_1 \\ \mp M/R_2 & -L_2/R_2\end{pmatrix}\frac{d}{dt}\begin{pmatrix}\delta I_1(t) \\ \delta I_2(t)\end{pmatrix}. \tag{14}$$

This equation can be in turn converted to the form of Eq. (11) by inverting the 2×2 induction matrix:

$$\frac{d}{dt}\begin{pmatrix}\delta I_1(t) \\ \delta I_2(t)\end{pmatrix} = \begin{pmatrix}-\frac{R_1}{L_1(1-k^2)} & \pm\frac{kR_2}{(1-k^2)\sqrt{L_1L_2}} \\ \pm\frac{kR_1}{(1-k^2)\sqrt{L_1L_2}} & -\frac{R_2}{L_2(1-k^2)}\end{pmatrix}\begin{pmatrix}\delta I_1(t) \\ \delta I_2(t)\end{pmatrix}. \tag{15}$$

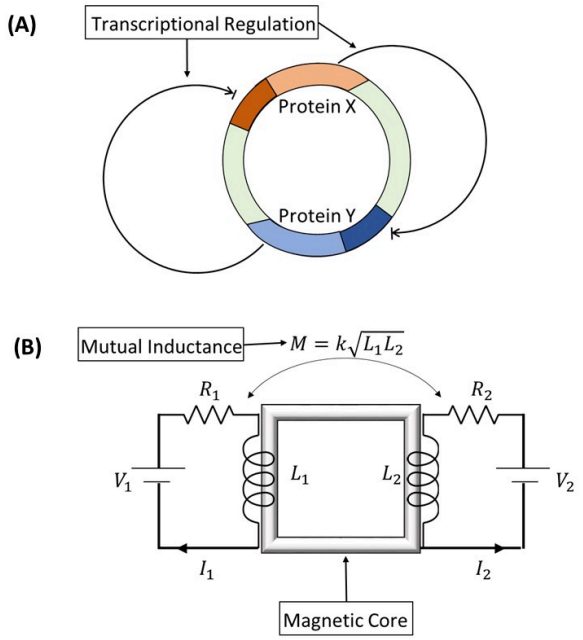

FIG. 2. Mutually regulating circuits. (A) A schematic representation of a plasmid circuit in which two genes act as transcriptional regulators for each other. The arrows indicate regulatory interactions, with the pointed arrowhead representing positive, promotional regulation, and the flat arrowhead representing negative, repressive regulation. (B) A schematic diagram of the equivalent magnetic circuit, which is a simple transformer. As drawn, the circuit is analogous to the case of mutual repression; the case of mutual promotion can be obtained by reversing the transformer polarity.

In the above, we have made use of the standard definition that $M \equiv k\sqrt{L_1L_2}$, where $0 \le k < 1$ is a coupling parameter gauging the strength of the inductive interactions between the circuits.

Although it is now clear how to relate the kinetic rate constants of the mutually regulating plasmid circuit to the parameters of the simple transformer circuit, there are a few irreconcilable differences between Eq. (11) and (15) that must be addressed. Perhaps most distressing is the fact that the matrix elements of the inverted induction matrix are all proportional to a factor of $(1-k^2)^{-1}$, which will cause them to diverge as $k \to 1$. This limit corresponds to a perfectly coupled transformer for which a fluctuation in the current of one circuit loop can cause an instantaneous adjustment in the current of the other. There is no meaning to Eq. (15) in this case because such a transformer has no dynamics. Although no such divergence is possible in Eq. (11), there is an analogous regime in the chemical kinetics case. Oftentimes short-lived chemical intermediates like enzyme-substrate complexes are approximated as existing always at steady state, even when the overall chemical system is not. This so-called quasi-steady state assumption (QSSA) results in the concentrations of enzyme and free substrate instantaneously determining at all times the concentration

of bound substrate.

A second important difference between the genetic and magnetic systems is that the plus/minus signs in Eq. (15) are determined by the polarity of the transformer, i.e., whether the two loop currents flow in the same or opposite directions. Because the magnetic induction between two current loops is always symmetric, these two signs cannot be chosen independently and must instead always be the same (both positive or both negative). In the genetic case, one could certainly construct a mutually regulating plasmid in which protein X positively regulates protein Y, but protein Y negatively regulates X. This places an important restriction on the regulatory topology of plasmid circuits to which our inductive analogy can be applied.

One final observation is that the stability condition $k_D k'_D > k_{XY} k_{YX}$ can be shown to reduce in the magnetic case to the condition $k^2 < 1$, which is, for real materials, always true. The fact that a transformer circuit cannot be dynamically unstable seems to suggest that we must also restrict our analogy to plasmid circuits whose dynamics consist of stable fluctuations about a single steady state; but, since our analogy is ultimately a mathematical and not a physical one, we are free to artificially choose $k > 1$, which converts the fixed point of the transformer circuit into a saddle point instability. In the conclusions section we will briefly outline how this can be used to extend our analogy to chemical systems with multiple steady states. As the next subsection will demonstrate, this kind of physically implausible but mathematically permissible manipulation will also be our means for introducing crosstalk into the magnetic system.

C. The Elastic Inductor

Our basic intuition for the impact crosstalk will have on relaxation kinetics is that an excess of protein will place a greater strain on the shared pool of cellular resources, resulting in a slower transition back to the homeostatic steady state. This effect has been observed experimentally, and it has been found that, far from a detriment, this slowdown is actually leveraged by some bacteria in beneficial ways. In the stress response network of *E. coli*, for example, a stress-induced increase in protein misfoldings places a strain on the limited supply of the clean-up protease enzyme ClpXP. This strain results in a depressed degradation rate of the sigma cofactor σ^S, which then accumulates and enhances the transcription rate of stress-reducing proteins [24].

We shall build this phenomonology into our magnetic circuits by exaggerating the magnitude of a second-order, nonlinear feedback mechanism that is peculiar to inductor coils. We begin by assuming that each inductor element in our circuits consists of a solenoid of length ℓ with N turns; but, as is standard in linear-circuit theory, we shall approximate the magnitude of the magnetic field B within this coil as if the inductor were an infinite solenoid

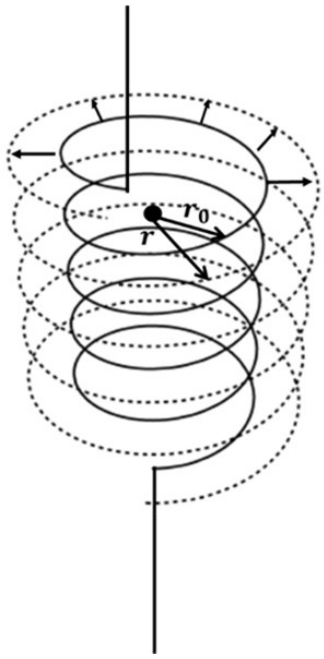

FIG. 3. Conceptual illustration of the elastic inductor. As current flows through the solenoid, a magnetic field is produced that exerts an outward Lorentz pressure on the coil. This causes it to expand radially, increasing the cross-sectional area of its turns and the total magnetic flux passing through the coil. This additional flux induces an even larger electromotive force to oppose any changes to the current, making the elastic inductor more slowly relaxing than a normal, rigid inductor–especially for larger currents.

with fixed turn density N/ℓ:

$$B = \frac{\mu_0 N I}{\ell}. \tag{16}$$

In the above, μ_0 is the permeability of free space and I is the current running through the coil. This current will cause each infinitesimal length element of the coil, $d\mathbf{s}$, to experience a Lorentz force, $d\mathbf{F}$, from the magnetic field generated by the rest of the inductor:

$$d\mathbf{F} = I d\mathbf{s} \times \mathbf{B}, \tag{17}$$

which points in the outward direction everywhere along the coil. The magnetic field in the above expression must be evaluated at the boundary between the inside and outside of the coil, where its strength, under our assumptions, discontinuously drops from the expression given in Eq. (16) to zero. For simplicity, we shall treat the strength of the field right at the boundary as the average of its values just inside the coil and just outside, which will make it equal to half the value of Eq. (16). Formally we must also subtract out the contribution of the B-field generated by the element $d\mathbf{s}$ itself, but this will make a negligible difference, since we have assumed that the element is infinitesimal in length.

Assuming the turns of the inductor coil are circular with radius r, we find that the total Lorentz pressure,

P_B, exerted on each turn is

$$P_B = \frac{\mu_0 N I^2}{2\ell}. \tag{18}$$

The elastic deformation caused by this pressure is negligibly small for most known conductive materials under sustainable current loads; but, for the purpose of introducing crosstalk into our magnetic circuit analogues, we shall perform a gedankenexperiment in which we conceive of an inductor that is both metallically conductive and sufficiently elastic to expand under its own Lorentz pressure (see the schematic in Fig. 3). For small deformations, we assume a linear stress-strain relation of the form:

$$P_B = E\left(\frac{r - r_0}{r_0}\right), \tag{19}$$

where E is the elastic modulus of the uniform expansion and r_0 is the radius of each coil loop in the absence of current. Solving this relation for r and substituting it into the expression for the total magnetic flux passing through the inductor, $\phi = \pi r^2 N B$, we ultimately find:

$$\phi = LI\left(1 + \frac{L}{\epsilon} I^2\right)^2. \tag{20}$$

In the above, the linear self-inductance is defined as $L \equiv \pi r_0^2 \mu_0 N^2/\ell$, and $\epsilon \equiv 2\pi r_0^2 N E$ is an elastic energy scale.

As conceptualized, the elastic inductor houses two linear processes: the induced current flowing through the coil grows linearly with the magnetic flux passing through its cross section (Faraday's law), and the extent of the coil deformation varies linearly with the Lorentz pressure. These processes are clearly not independent of one another, as the magnetic flux is a function of the square of the coil radius, and the Lorentz pressure depends upon the square of the current. The result of this nonlinear interdependence is a slowdown in the relaxation of the current back to its steady value: a reduction in current results in a larger change in magnetic flux, due to the larger cross-sectional area of the elastically expanded coil, and this drives a larger electromotive force to oppose the change in current. This effect will be exacerbated for larger currents, consistent with our expectation that larger protein concentrations will cause a greater resource strain in the cellular context.

Thus far we have restricted our considerations to how cellular crosstalk will impact the relaxation of protein expression levels back towards steady state after a perturbation, but the sharing of limited resources will also shift the position of the steady state itself [12, 23]. However, since our kinetics model is derived from a linear order expansion about steady state, the actual values of the steady protein concentrations are irrelevant and can always be set at experimentally verified levels through appropriate choices of the model parameters.

III. RESULTS AND DISCUSSION

We proceed to examine how elastifying the inductor coils in the magnetic circuits of the previous section (see Figs. 1(B) and 2(B)) modifies their dynamic current profiles. In each case we relate the dynamics to what one would anticipate from the analogous plasmid system, and we then complete the analogy by devising sets of coupled elementary reactions whose kinetics schematically reproduce this behavior.

A. Schematic Model for Protease-mediated Catabolism

To assess the impact of placing our hypothetical elastic inductor into the RL-circuit loop of Fig. 1(B), we must determine how the circuit voltage will drop across it. Faraday's law should still hold, so the voltage drop should equal the time derivative of the flux. The difference is that instead of the flux depending linearly on the current as $\phi = LI$, the flux through the elastic inductor will be related nonlinearly to the current through Eq. (20). Differentiating that equation with respect to time, we can then proceed to use the Kirchhoff Voltage Law to derive a differential equation for the dynamic current profile of the circuit:

$$\frac{dI(t)}{dt} = \frac{V - RI(t)}{L\left(1 + \frac{L}{\epsilon} I(t)^2\right)\left(1 + \frac{5L}{\epsilon} I(t)^2\right)}. \tag{21}$$

The numerator of the right-hand side ensures that $I = V/R$ is still a stable fixed point of the system, but the denominator will cause the relaxation time of the circuit to grow monotonically with the current. This assessment is borne out in Fig. 4, where we have solved Eq. (21) numerically and plotted its current profile for two different initial conditions. The corresponding dashed lines of each color represent the relaxation of the standard RL-circuit loop. As surmised, the feedback of the elastic inductor retards the relaxation for all currents, but the relaxation is asymmetric about steady state, relaxing far more slowly from above than from below. We now argue that this behavior is precisely what we would anticipate as the leading order impact of cellular crosstalk on the analogous gene circuit in Fig. 1(A).

In our assessment of the kinetics of this plasmid circuit (see Eq. (5)), we treated the degradation of the protein concentration as a Poisson process, with every protein behaving like an unstable radioactive isotope, modeled to spontaneously decay at any moment with frequency k_D. In reality, the degradation or *catabolism* of each protein molecule is facilitated by an enzyme called a protease. Because the variety of proteins in a cell far exceeds the number of different protease enzymes, each type of protease is responsible for catabolizing many different proteins. This resource-sharing of a finite protease pool across multiple protein populations will universally

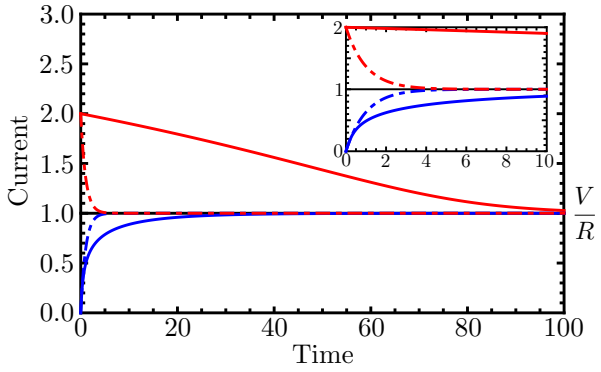

FIG. 4. The time-dependent current profile of the elastified RL-circuit for two different initial conditions, one above the steady-state current V/R (in red) and one below it (in blue). All parameter values (V, R, L, etc.) were set to unity for simplicity. Dashed lines indicate the behavior of the standard RL-circuit initialized from the same two initial conditions (in matching colors). The inset plots the same curves over a shorter time scale to better illustrate the exponential decay of the standard circuit.

depress the relaxation of $[X]_t$ back to steady state, and this kinetic slowdown will be more acute when there are more X molecules to strain the protease population. This is, of course, precisely the dynamic behavior described by Eq. (21).

Crosstalk should also have an effect on the transcription rate of protein X, which we assumed to be constant in our previous analysis. In fact, we expect that this rate should fluctuate as a function of the availability of RNA polyermase and other shared transcription initiation factors. As we shall see shortly, reproducing the nonlinear dynamics of Eq. (21) will require us to account for variability in both the transcription and degradation rates of protein X.

While it is possible to construct a sequence of elementary reactions that exactly reproduce the functional form of Eq. (21), the result is not terribly illuminating. Since we only really wish to schematically reproduce the phenomenology of asymmetric relaxation, we will instead aim for a simpler functional target:

$$\frac{d[X]_t}{dt} = \frac{V_{max}\,(k_X - k_D[X]_t)}{1 + K_A[X]_t^n}, \tag{22}$$

where $n \geq 2$ and V_{max} and K_A are constants (with appropriate units to make the above dimensionally correct). Aside from the factor in the numerator that stabilizes the system at the desired steady-state concentration of k_X/k_D, the above is essentially a Hill function [25], which is frequently employed in modeling enzyme kinetics.

A set of elementary chemical reactions whose overall kinetics can be described by Eq. (22) is straightforward to construct:

$$\begin{aligned} \mathrm{X} + \mathrm{S} &\underset{\mathrm{k_X}}{\overset{\mathrm{k_D}}{\rightleftharpoons}} \mathrm{S} \\ \mathrm{nX} + \mathrm{S} &\underset{\mathrm{k_-}}{\overset{\mathrm{k_+}}{\rightleftharpoons}} \mathrm{SX}_n \quad \text{(QSSA)}. \end{aligned} \tag{23}$$

Note that the latter pair of reactions is assumed to equilibrate so rapidly that it can be treated as always being at a quasi-steady state. It then follows that $V_{max} = [S]_{tot}$, where $[S]_{tot} \equiv [S]_t + [SX_n]_t$ is presumed to be a constant independent of time, and $K_A = k_+/k_-$.

Our desire to reproduce the behavior of Eq. (21) in the schematic form of Eq. (22) forced us to introduce a virtual chemical species S into the kinetics. This species can be identified as a protease enzyme by the forward reaction $\mathrm{X} + \mathrm{S} \longrightarrow \mathrm{S}$, but the reverse reaction simultaneously identifies it as RNA polymerase or some other transcription initiator that constituitively controls the transcription of X. This dual identification is not problematic, since S is ultimately a mathematical construct used to phenomenologically account for the impact of crosstalk on the kinetics of X. The remaining pair of reactions use the formation of a virtual complex SX_n to model S as a limited resource. There will always be some fraction of S that is busy degrading other proteins, and we represent this fraction as $[SX_n]$. Note that this concentration will tend to grow with $[X]$, thereby modeling the strain the X population places upon the protease pool.

While introducing a virtual molecular population might seem troubling at first blush, it must be emphasized that by doing so we have succeeded in phenomonologically capturing the impacts of two different types of crosstalk on the kinetics of the protein of interest with only a marginal increase in mathematical complexity. It remains to be seen how accurately this schematic model can be fit to data from real biological systems, and the experiments required to make that assessment will be discussed in the conclusions section.

B. Schematic Model for Crosstalk-driven Tristability

We next consider the effect of elastifying the inductors in the simple transformer circuit of Fig. 2(B). In addition to the flux-current relation of Eq. (20), we also need to know how the magnetic flux through one inductor coil will be affected by the current running through the other. In the standard transformer circuit, this relation would be linear: $\phi_{12} = MI_2$, where ϕ_{12} is the contribution to the flux through inductor 1 as a result of the current in inductor 2. In the elastic transformer, the flux through one coil depends on the magnetic field generated by the other coil as usual, but now it also depends upon the first coil's cross-sectional area. The result is that the magnetic flux through one coil depends linearly on the other coil's

current but nonlinearly upon its own current:

$$\phi_{12} = M I_2 \left(1 + \frac{L_1}{\epsilon_1} I_1^2\right)^2 . \tag{24}$$

Note that quantities like L_1 are now formally defined in terms of the permeability μ of the ferromagnetic material around which each solenoid is wrapped rather than the permeability of free space μ_0, and we have further assumed that the enwrapped ferromagnetic material expands and contracts so as to always fill the interior of each solenoid, without impacting the material's magnetic properties.

Applying the Kirchhoff Voltage Law to the elastic transformer circuit thus yields the following coupled pair of equations:

$$\begin{aligned} V_1 = \left(1 + \frac{L_1}{\epsilon_1} I_1^2\right) \Bigg\{ \left[L_1 \left(1 + \frac{5L_1}{\epsilon_1} I_1^2\right) \pm M \frac{4L_1}{\epsilon_1} I_1 I_2 \right] \frac{dI_1}{dt} \\ \pm M \left(1 + \frac{L_1}{\epsilon_1} I_1^2\right) \frac{dI_2}{dt} \Bigg\} + R_1 I_1 \\ V_2 = \left(1 + \frac{L_2}{\epsilon_2} I_2^2\right) \Bigg\{ \left[L_2 \left(1 + \frac{5L_2}{\epsilon_2} I_2^2\right) \pm M \frac{4L_2}{\epsilon_2} I_1 I_2 \right] \frac{dI_2}{dt} \\ \pm M \left(1 + \frac{L_2}{\epsilon_2} I_2^2\right) \frac{dI_1}{dt} \Bigg\} + R_2 I_2 . \end{aligned} \tag{25}$$

In the above, the time argument of the currents has been suppressed for compactness. As with Eq. (13), the $\pm$ signs must all be either plus or minus. This sign choice results in only minor differences to the phase portrait of the standard transformer circuit, due to its guaranteed dynamic stability, but polarity has a much more pronounced effect on the behavior of the elastic transformer.

In the case where the plus signs are chosen in Eq. (25), corresponding to the two RL-circuits of the transformer having their currents rotating in the same direction, the pair of equations can be algebraically solved for the time derivatives of the currents, and a representative phase portrait of this system is plotted in Fig. 5(A). This portrait exhibits a single, stationary fixed point at the steady state $(I_1, I_2) = (V_1/R_1, V_2/R_2)$; however, just as with the single, elastic RL-circuit, relaxation back to this steady-state is dramatically slower from above than from below. This leads to four distinct dynamical regimes.

When both currents fluctuate below their steady values (lower-left quadrant of the phase plot), the relaxation trajectories curve inwards, decaying in an exponential-like fashion back towards the fixed point. When one current fluctuates below and the other above (upper-left and lower-right quadrants), the return trajectories bend into L-shapes, relaxing completely in one direction before having substantially relaxed in the other. Finally, when both currents fluctuate above their steady-state values (upper-right quadrant), the phase curves bow outwards, and inductive feedback greatly frustrates the return to equilibrium for both loop currents.

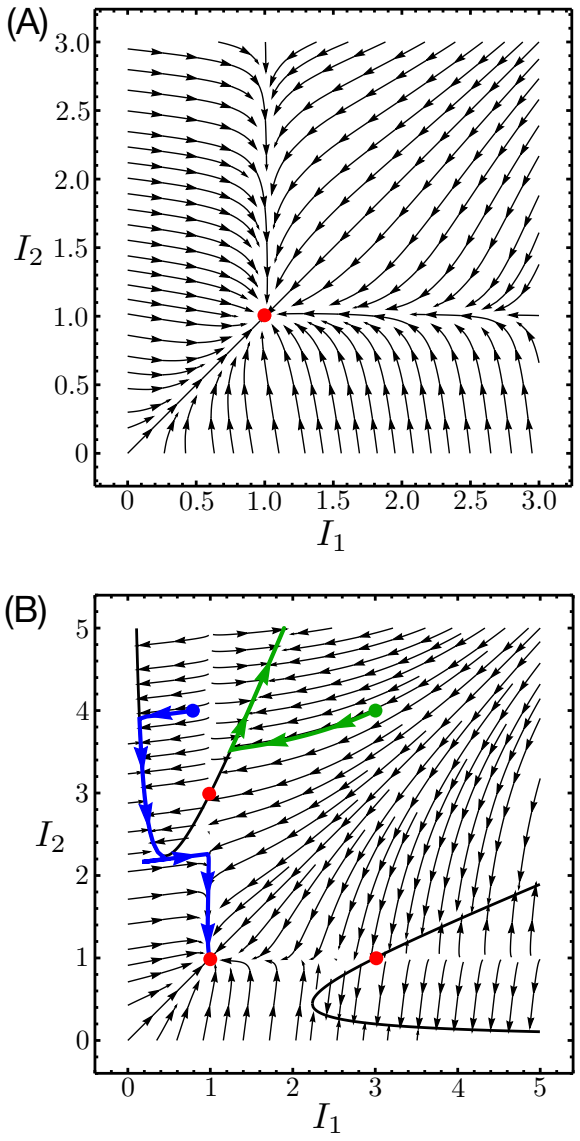

FIG. 5. Phase portraits of the elastic transformer. (A) A dynamical phase portrait for the elastic transformer circuit in the case where the two loop currents rotate in the same direction. All parameters were set equal to unity for convenience, except for the coupling parameter k, which was set equal to 1/2. The red dot at $(I_1, I_2) = (1, 1)$ marks the single, stable fixed point of the system. (B) For the same set of parameter values, the phase portrait for the oppositely polarized elastic transformer is plotted. The same stable fixed point exists, but now there are two additional saddle points that lie along the curves defined by the sets of current values that reduce one or the other of the bracketed terms in Eq. (25) to zero. Two phase trajectories that illustrate the behavior of the dynamics near these curves are plotted in green and blue, illustrating, respectively, how these saddle points either deflect the currents away towards a trivial fixed point at infinity or back towards the stable fixed point at $(1, 1)$.

If the minus signs are instead chosen in Eq. (25), solving for the current derivatives is complicated by the fact

that the quantity in the square brackets in each equation can now be zero. The bracketed term in the first equation, for example, is a quadratic polynomial in the current I_1 that will be zero under the following conditions:

$$\begin{aligned} I_1(t) &= \frac{2M}{5L_1} I_2(t) \pm \sqrt{\frac{4M^2}{25L_1^2} I_2(t)^2 - \frac{\epsilon_1}{5L_1}} \\ &\equiv I_{1\pm}(t) \\ I_2(t) &> \frac{1}{2}\left(\frac{5L_1\epsilon_1}{M^2}\right)^{1/2}. \end{aligned} \tag{26}$$

The inequality in the above is required to make $I_{1\pm}(t)$ a real-valued current. Substituting $I_1 = I_{1\pm}$ back into the first equation of Eq. (25), we get the following differential equation:

$$\frac{dI_2(t)}{dt} = \frac{R_1 I_{1\pm}(t) - V_1}{M\left(1 + \frac{L_1}{\epsilon_1} I_{1\pm}(t)^2\right)^2} \tag{27}$$

Note that since $I_{1\pm}$ is a function of I_2 alone, this differential equation is uncoupled from the dynamics of I_1 and can be solved independently. The resultant dynamics of $I_2(t)$ then define those of $I_1(t)$ through Eq. (26). The functional form of Eq. (27) also makes it clear that this system has an additional fixed point when $I_{1\pm} = V_1/R_1$. A similar analysis can be performed if instead it is the square-bracketed term in the expression for V_2 that is zero, and analogues to Eqs. (26) and (27) that swap the indices 1 and 2 are the result. It is not possible for both bracketed terms to be zero simultaneously.

The corresponding phase portrait for this choice of polarization is plotted in Fig. 5(B) for the same parameter values as in panel (A). For most values of the currents, the vector field $(dI_1/dt, dI_2/dt)$ is determined by algebraically inverting Eq. (25). For values that fulfill either Eq. (26) or its index-swapped analogue, however, the dynamics are constrained to one of two convex curves, each of which contains a hyperbolic fixed point. These special curves actually serve as attractors for large swaths of the phase portrait, with trajectories along one side of the fixed point ultimately being funneled back towards the stable fixed point at $(I_1, I_2) = (V_1/R_1, V_2/R_2)$ and those along the other getting shunted off towards infinity. Representative trajectories illustrating these two dynamical outcomes are highlighted in the figure. They were computed by numerically integrating Eq. (25) with a time step of $\Delta t = 0.1$, taking care to switch to using Eqs. (26) and (27) for time intervals where the trajectory follows the convex curve they define.

When the loop currents of the elastic transformer rotate in the same direction, the negative feedback mechanism of each elastic inductor synergizes with the other to frustrate the relaxation dynamics even further; when the currents flow in opposite directions, the individually negative feedback mechanisms actually provide positive feedback to one another, making it possible for the entire system to become destabilized when $I_1 > V_1/R_1$ and $I_2 \gg V_2/R_2$ (or vice versa). This destabilization drives both currents towards infinity, leading to circuit failure or overload. Even for arbitrarily large currents, however, stability will be maintained so long as $(V_2/R_2)I_1 \approx (V_1/R_1)I_2$, although the competition between stabilizing negative and destabilizing positive feedback results in the already slow relaxation dynamics of each elastic inductor becoming even slower.

The divergent behavior of the elastic transformer seems to disqualify it as a model for cellular crosstalk, since it is hard to imagine mutual transcriptional regulation driving unbounded growth; but recall that our analogy between genetic and magnetic circuits was predicated upon an assumption of linearized chemical kinetics near steady state. Concentrations that diverge away from their steady-state values violate that assumption of linear stability, invalidating our analogy in the problematic region of the phase portrait of Fig. 5(B). Of course, if our analogy between magnetic and genetic crosstalk is to have any value, this breakdown in linearity must al least be assigned some plausible physical significance in our biochemical system.

The oppositely polarized transformer configuration is equivalent to mutual transcriptional repression in our analogy, and the genetic circuit consisting of two genes whose encoded proteins X and Y repress each other's transcription can be shown to behave as a so-called "genetic toggle switch" when the kinetics of repression are sufficiently nonlinear [26]. Essentially, when the maximal rate of repression is weak, the system exhibits a single stable fixed point for $\langle[X]\rangle = \langle[Y]\rangle$ (assuming symmetric repression rates); but when the repression rate passes a critical threshold, the original stable fixed point becomes unstable, pushing the concentrations towards one of two new stable fixed points–one for which $\langle[X]\rangle > \langle[Y]\rangle$ and the other for which $\langle[Y]\rangle > \langle[X]\rangle$. Appropriate inducers can then be used to push the system from one of these fixed points to the other–hence the reason for calling this gene circuit a toggle switch.

Phenomenologically, the two phase portraits in Fig. 5 resemble this kind of switch from a unimodal to a multimodal system, where the true nonlinear kinetics would have to move the two attractors at infinity in Fig. 5(B) to finite positions within the phase portrait. Since the original fixed point remains stable in both cases and merely has its basin of attraction circumscribed in the latter, this system would be a tristable switch. A more crucial difference here is that the transition between the number of fixed points is not achieved by smoothly tuning the coupling strength between the two circuits, but rather by flipping their relative polarity. The character of transcriptional regulation, i.e., promoting versus inhibiting interactions, is set by the biology of the system and cannot be toggled freely. Consequently, the tristability of the repressive circuit should be understood instead as a fundamental consequence of the nonlinearities imposed on the kinetics by crosstalk.

We emphasize that at this point we are merely spec-

ulating that tristability is the most plausible biochemical interpretation of the divergences observed in Fig. 5(B), but this speculation is supported by the findings of more biologically detailed models of transcriptional circuits that have previously identified crosstalk as a potential source of multistability [27, 28]. Experimental evidence that crosstalk can specifically cause a unimodal system to become trimodal has even been found for a synthetic gene circuit inoculated into the bacterium *Escherichia coli* [29].

In order to devise a set of elementary chemical reactions that schematically reproduce the behavior of Eq. (25), we once again make some helpful simplifications. By neglecting crossterms proportional to $I_1 I_2$ as well as any terms of order M^2, we can invert Eq. (25) into the following form:

$$\frac{dI_1}{dt} = \underbrace{\frac{V_1 - R_1 I_1}{L_1\left(1+\frac{L_1}{\epsilon_1}I_1^2\right)\left(1+\frac{5L_1}{\epsilon_1}I_1^2\right)}}_{\text{Circuit 1}} \mp \frac{M\left(1+\frac{L_1}{\epsilon_1}I_1^2\right)}{L_1\left(1+\frac{5L_1}{\epsilon_1}I_1^2\right)} \underbrace{\frac{V_2 - R_2 I_2}{L_2\left(1+\frac{L_2}{\epsilon_2}I_2^2\right)\left(1+\frac{5L_2}{\epsilon_2}I_2^2\right)}}_{\text{Circuit 2}}. \tag{28}$$

In the above, the time dependence of the currents has been suppressed for compactness and the rate law for I_2 has exactly the same form but with the indices 1 and 2 swapped. This simplified form is appealing because it explicitly contains the contributions of the two individual elastified RL-circuits (as given by Eq. (21)).

In the mutually repressive case, we can recover some of the divergent character of the exact phase portrait by creatively reducing Eq. (28) to the following schematic rate law, now expressed in chemical kinetics terms:

$$\frac{d[X]_t}{dt} = \frac{V_{max}(k_X - k_D[X]_t)}{1 + K_A[X]_t^n} + \frac{U_{max}(1+K_A[X]_t^n)(k_Y - k_D[Y]_t)}{1+Q_A[Y]_t^m}. \tag{29}$$

The corresponding differential equation for $[Y]_t$ is:

$$\frac{d[Y]_t}{dt} = \frac{V'_{max}(k_Y - k_D[Y]_t)}{1 + Q_A[Y]_t^m} + \frac{U'_{max}(1+Q_A[Y]_t^m)(k_X - k_D[X]_t)}{1+K_A[X]_t^n}. \tag{30}$$

A representative phase portrait for this system of equations is plotted in Fig. 6, demonstrating that this schematic model retains the phenomenology of a centrally stable region where $[X] \approx [Y]$ flanked by two unstable regions for $[X] \gg [Y]$ and $[Y] \gg [X]$.

We sensibly expect the kinetics of this system to reduce, in the absence of coupling, to the rate law given

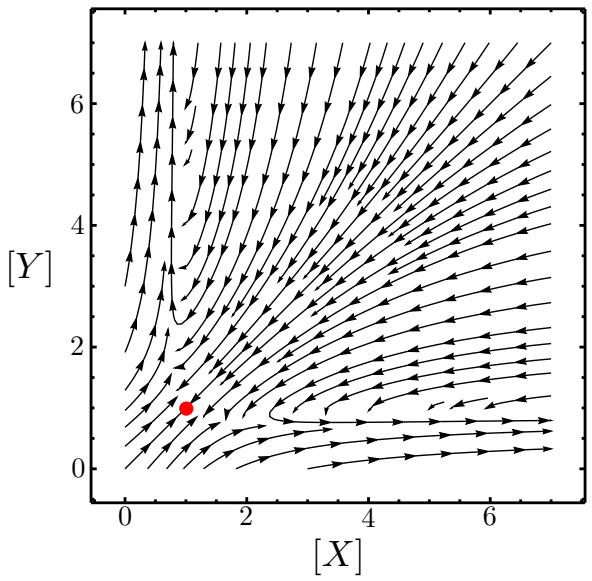

FIG. 6. Phase portrait of the mutually regulating plasmid circuit with crosstalk. The dynamical phase portrait defined by Eqs. (29) and (30) is plotted for $U_{max} = U'_{max} = 1/2$ and all other parameters equal to unity (an equivalent parameter set to that used for the phase portraits in Fig. 5). Once again, the red dot marks the fixed point at $(1, 1)$.

by Eq. (22), meaning that the elementary reactions that lead to Eq. (29) must, at bare minimum, include:

$$\begin{aligned}
&\mathrm{X} + \mathrm{S} \underset{\mathrm{k_X}}{\overset{\mathrm{k_D}}{\rightleftharpoons}} \mathrm{S} \\
&\mathrm{nX} + \mathrm{S} \underset{\mathrm{k_-}}{\overset{\mathrm{k_+}}{\rightleftharpoons}} \mathrm{S\,X}_n \quad \text{(QSSA)} \\
&\mathrm{Y} + \mathrm{Q} \underset{\mathrm{k_Y}}{\overset{\mathrm{k_D}}{\rightleftharpoons}} \mathrm{Q} \\
&\mathrm{mY} + \mathrm{Q} \underset{\mathrm{q_-}}{\overset{\mathrm{q_+}}{\rightleftharpoons}} \mathrm{Q\,Y}_m \quad \text{(QSSA)}.
\end{aligned} \tag{31}$$

In addition to the above, the coupling between proteins X and Y will be mediated through the additional set of reactions:

$$\begin{aligned}
&(QSSA)\begin{cases} \mathrm{Q} \xrightarrow{\mathrm{q_A}} \mathrm{Q} + \mathrm{A} \\ \mathrm{SX}_n + \mathrm{A} \xrightarrow{\mathrm{k_A}} \mathrm{SX}_n \end{cases} \\
&(QSSA)\begin{cases} \mathrm{S} \xrightarrow{\mathrm{q_B}} \mathrm{S} + \mathrm{B} \\ \mathrm{QY}_m + \mathrm{B} \xrightarrow{\mathrm{k_B}} \mathrm{QY}_m \end{cases} \\
&\mathrm{nX} + \mathrm{A} \xrightarrow{\mathrm{k_Y}} (\mathrm{n}+1)\,\mathrm{X} + \mathrm{A} \\
&\mathrm{nX} + \mathrm{Y} + \mathrm{A} \xrightarrow{\mathrm{k_D}} (\mathrm{n}-1)\,\mathrm{X} + \mathrm{Y} + \mathrm{A} \\
&\mathrm{mY} + \mathrm{B} \xrightarrow{\mathrm{k_X}} (\mathrm{m}+1)\,\mathrm{Y} + \mathrm{B} \\
&\mathrm{mY} + \mathrm{X} + \mathrm{B} \xrightarrow{\mathrm{k_D}} (\mathrm{m}-1)\,\mathrm{Y} + \mathrm{X} + \mathrm{B}.
\end{aligned} \tag{32}$$

Though not immediately obvious, the above collection of elementary reactions do indeed produce the

rate laws of Eq. (29) and (30), with $K_A \equiv k_+/k_-$, $Q_A \equiv q_+/q_-$, $V_{max} \equiv [S]_{tot}$, $V'_{max} \equiv [Q]_{tot}$, $U_{max} \equiv (q_A/k_A)([Q]_{tot}/[S]_{tot})$, and $U'_{max} \equiv (q_B/k_B)([S]_{tot}/[Q]_{tot})$. This looks rather complicated and arbitrary, but the four virtual species we have introduced all have reasonable interpretations.

The proteins S and Q may still be interpreted dually as both transcription initiators and protein degraders, and the first set of bracketed reactions in Eq. (32) indicate that species A represents one of the other proteins transcribed by Q that S also degrades. Note that it is SX_n that degrades A because SX_n is the fraction of S not occupied with the degradation or transcription of X. The species B is, analogously, a virtual species transcribed by S and degraded by Q (in the form QY_m). Both virtual species A and B are assumed to exist in a quasi-steady state.

The remaining two reactions involving A describe its role as an intermediary for the regulation of X by Y. The species A is assumed to be a transcription factor for X, and Y is modeled as repressing the transcription of X principally by interfering with the binding of A. The virtual species S is still the principal promoter of X transcription, so the promoter site for protein X will only be vacant for A or Y to bind if the concentration of X is large, in which case S will be tied up acting in its role as protease. This restriction is enforced by including nX on the left-hand side of both reactions. The species B promotes Y in an analogous manner and this process is similarly frustrated by X.

IV. CONCLUSIONS

In this paper, we have established a mathematical analogy between the linearized kinetics of mutually regulating plasmid circuits near homeostasis and the current dynamics of inductively interacting magnetic circuits. Within this analogy, a protein concentration near steady state is represented as a simple RL-circuit loop, and the transcriptional regulation of two such proteins by each other is represented by inductively coupling two RL circuits by a loop of ferromagnetic material, as in a transformer. By itself, this analogy is not terribly remarkable, as nearly all physical systems exhibit similar phenomenology when linearized about a stable fixed point in their dynamics. What is noteworthy, however, is the manner by which we meaningfully translate a nonlinear feedback mechanism introduced into the magnetic system into a schematic kinetic theory for the influence of crosstalk on the stability of a cell's biochemical state that does not explicitly depend upon knowing the dynamic concentrations of shared biomolecular resources. Instead, our model introduces virtual chemical species whose presumed quasi-steady total concentrations serve as free parameters that modulate the strength of the crosstalk interactions.

For a plasmid circuit with a single, constitutively regulated gene, we predict that its steady-state concentration should relax at vastly different rates depending upon whether the relaxation is driven by further transcription of the gene or by protein catabolism. This is consistent with the fact that most transcription factors, which regulate the rate of the former process, typically only influence the production rates of a small number of different genes whereas protease enzymes, responsible for the latter process, degrade a large number of different gene products. As a result, we expect the protease supply of a cell to be more susceptible to crosstalk and, consequently, the degradation of a protein excess to be much slower than the recovery from a protein deficiency. Our analogy suggests that we can model this asymmetry by introducing a single virtual molecular species into the model, which acts simultaneously as a transcriptional promoter and a protease enzyme, the precise stoichiometry of which can be used to tune the sensitivity of the kinetics to fit experimental measurements.

For a plasmid circuit consisting of two mutually repressive genes, we predict that crosstalk can prevent the system from relaxing back to steady state at all if the concentration of one gene product becomes too much larger than the other. Because the nonlinear contributions to the model in this case violate our initial assumption of linear stability, we cannot predict precisely what becomes of the diverging trajectories, but it is reasonable to assume they eventually reach new steady states. This implies that resource limitations can render cells more adaptable, able to switch between different biochemical states depending upon how metabolic constraints impact transcriptional rates. For this system, our analogy requires we introduce two virtual species for each gene product (four in total), with one species of each pair governing the crosstalk experienced from constitutive regulation and catabolism (as in the previous case) and the other characterizing the crosstalk associated with mutual regulation.

Although our analogy between genetic and magnetic circuits succeeds in reproducing much of our intuition about how crosstalk should modulate gene regulation, there are some fundamental incompatibilities between the biochemistry of the former and the physics of the latter that still need to be addressed. For starters, the inherent symmetry of inductively coupled circuits seems to preclude the extension of the analogy to a broad class of plasmid circuits that are not mutually regulating or that have mutual but asymmetric regulation, e.g., when protein X promotes transcription of protein Y, but Y represses transcription of X. Since the elastic inductor formalism we devised was merely a mathematical construct used to incorporate crosstalk into our magnetic circuits, with no regard for whether such a component was physically realizable, we could conceivably address this limitation by introducing another fictitious component, such as a ferromagnetic loop that only permits magnetic flux to flow in one direction. While physically unreasonable, such a construct might mathematically allow for asym-

metrically coupled RL-circuit loops that could then map, through our analogy, to gene circuits with unidirectional regulation.

A second issue is the fact that linear circuit theory has constrained our analogy to focus on dynamics close to steady state, even though many plasmid circuits of interest have dynamic behavior that switches or oscillates between multiple stable fixed points. While one solution might be to account for the higher order nonlinearities in the electromagnetic circuit components, there is no guarantee that our analogy with chemical kinetics will hold up beyond linear order. A better solution is to do what one often does with complex, nonlinear systems and simply perform a separate linearization about each fixed point. Once the dynamic behavior near each fixed point is characterized, one can typically predict, at least qualitatively, how the system will behave in the regions in between. The fundamental stability of transformer circuits would seem to make the characterization of the dynamics near an unstable fixed point untenable, but this can be resolved, as described earlier, by artificially choosing an inductive coupling parameter $k > 1$.

A final drawback of note derives from the fact that chemical kinetics is really only valid for descriptions of large systems where discrete numbers of proteins can be approximated as continuous concentrations. The transcriptional regulation within a single cell is often better modeled by discrete, stochastic master equations, which only map to the continuous, deterministic rate laws of chemical kinetics under certain circumstances (such as when averaged over a large cellular population). While it is straightforward to use the same set of elementary reactions to build either a discrete or a continuous chemical model, the same cannot be said for a magnetic circuit. While it is true that the continuous currents we have identified as being analogous to protein concentrations do in fact arise from the stochastic transport of discrete charge carriers, there is a vast difference in scale between a microscopic electron and a macroscopic circuit that is not present in the biological context, where both discrete and continuous models describe microscopic processes. There is no obvious solution to this paricular weakness of our analogy, other than to be grateful that most experimental measurements of protein expression are done at the population level, where chemical kinetics provides a reasonable description of expression profiles.

While the schematic kinetic models of resource-limited crosstalk that we have derived make seemingly reasonable predictions, their true sensibility must be validated experimentally. Ideally, what we want to analyze is a bacterial population in homeostasis, i.e., steady state, that has been inoculated with a plasmid circuit with several important characteristics. First, we want the principal gene product of the plasmid to be a fluorescent protein whose concentration can be measured at different times with optical microscopy. Second, we want the transcription rate of the plasmid to be dependent upon the external concentration of an inducer or inhibitor, so that the experimentor has a means of pushing the protein concentration away from its stable equilibrium value. Pulsing this system with inducer, for example, and subsequently measuring the amount of fluorescence in the population at several later times would provide relaxation data that could be directly compared with the predictions of our model (specifically Eq. (22)).

The second constraint is easily met. The well-known promoter pBAD, for example, can be leveraged to produce green fluorescent protein (GFP) at a rate that can be manipulated by varying the concentration of the sugar arabinose present in the bacterial medium [30, 31]. Maintaining a cellular population in a homeostatic steady state, on the other hand, presents a much greater obstacle. When grown withinin a Petri dish or some other finite volume of nutrient-rich medium, for example, a bacterial population will eventually saturate at a stationary level as its food source dwindles [32], but this so-called "stationary" phase is a resource-starved survival state, and is not representative of truly homeostatic behavior [33, 34], preceding a precipitous population crash once the pool of nutrients is fully depleted.

A long-lived steady state *can* be achieved within a cellular population, however, by using the microfluidic chemostat known colloquially as a mother machine [35]. In this device, cells are grown within channels so narrow that they are roughly constrained to lie in single file. Once a channel is full, the addition of a new cell through mitosis will force the topmost cell out of the channel into a wider, perpendicular channel where it will be whisked away by a constant flow of fresh medium. This medium, meanwhile, can diffuse through the sidechannels to provide a continuous source of nutrients to the cells. Only the "mother" cell at the very bottom of each channel will be in a true state of homeostasis, since its proximity to the feeding channel will never change; but, so long as the mother machine has a large number of growth channels, the set of mother cells can be treated as the homeostatic population whose time-resolved fluorescent expression can be measured.

If the basic phenomenology of our crosstalk model can be validated in the laboratory, then our framework can be extended to predict the resource-limited dynamics of more complex plasmid circuits. For any such circuit, our approach requires a reasonable model of its isolated chemical kinetics as input. After identifying the fixed points of the presumably nonlinear kinetics, one would then linearize the dynamics about each fixed point and determine the topology of the analogous magnetic circuit. After elasitifying the inductors in this circuit, one would then analyze the nonlinear current dynamics near each fixed point and map those behaviors schematically to sets of elementary chemical reactions. Note that while in reality crosstalk would also shift the positions of the fixed points, that is something we would account for when fitting the parameters of the model to experimental data. For simply predicting the overall performance of the gene circuit, however, we would merely need to combine the

nonlinear phase portraits near each fixed point to predict the possible phase trajectories of the entire system for various initial conditions.

ACKNOWLEDGMENTS

The theories described and the resulting data presented herein, unless otherwise noted, were obtained from research conducted under the Environmental Quality Installations Program of the U.S. Army Corps of Engineers by the U.S. Army Engineer Research and Development Center (ERDC). The authors express gratitude to Dr. Elizabeth Ferguson, Technical Director of the U.S. Army ERDC Installations and Operational Environment Research and Development Area, for support of this research. Opinions, interpretations, conclusions, and recommendations are those of the authors and are not necessarily endorsed by the U.S. Army.

[1] J. Hasty, D. McMillen, and J. J. Collins, Nature **420**, 224-230 (2002).
[2] D. Sprinzak and M. B. Elowitz, Nature **438**, 443-448 (2005).
[3] J. C. D. Ricci and M. E. Hernández, Critical Reviews in Biotechnology **20**, 79-108 (2000).
[4] T. Suganuma and J. L. Workman, Cell **135**, 604-607 (2008).
[5] C. K. Mapendano, S. Lykke-Andersen, J. Kjems, E. Bertrand, and T. H. Jensen, Molecular Cell **40**, 410-422 (2010).
[6] J. J. Faith, B. Hayete, J. T. Thaden, I. Mogno, J. Wierzbowski, G. Cottarel, S. Kasif, J. J. Collins, and T. S. Gardner, PLoS Biol. **5**, e8 (2007).
[7] A. Varma and B. O. Palsson, Applied and Environmental Microbiology **60**, 3724-3731 (1994).
[8] D. S.-W. Ow, D.-Y. Lee, M. G.-S. Yap, and S. K.-W. Oh, Biotechnol. Prog. **25**, 61-67 (2009).
[9] S. B. Lee, A. Seressiotis, and J. E. Bailey, Biotechnology and Bioengineering **27**, 1699-1709 (1985).
[10] W. E. Bentley and D. S. Kompala, Biotechnology and Bioengineering **33**, 49-61 (1989).
[11] A. Y. Weiße, D. A. Oyarzún, V. Danos,and P. S. Swain, PNAS **112**(9), E1038-E1047 (2015).
[12] Y. Qian, H. H. Huang, J. I. Jiménez, and D. Del Vecchio, ACS synthetic biology **6**(7), 1263-1272 (2017).
[13] M. B. Elowitz and S. Leibler, Nature **403**, 335-338 (2000).
[14] J. Garcia-Ojalvo, M. B. Elowitz, and S. H. Strogatz, PNAS **101**, 10955-10960 (2004).
[15] L. Potvin-Trottier, L., N. D. Lord, G. Vinnicombe, and J. Paulsson, Nature **538**, 514-517 (2016).
[16] B. Wang, R. I. Kitney, N. Joly, and M. Buck, Nature Comm. **2**, 508 (2011).
[17] T. S. Moon, C. Lou, A. Tamsir, B. C. Stanton, and C. A. Voigt, Nature **491**, 249-253 (2012).
[18] V. Hsiao, Y. Hori, P. W. K. Rothemund, and R. M. Murray, Mol. Syst. Biol. **12**, 869 (2016).
[19] G. De Rubertis and S. W. Davies, Proceedings of the IEEE-EMBS Special Topic Conference on Molecular, Cellular and Tissue Engineering, 145-146 (2002).
[20] K. W. Kohn and M. I. Aladjem, Mol. Syst. Biol. **2**(1), 2006-0002 (2006).
[21] R. Daniel, S. S. Woo, L. Turicchia, and R. Sarpeshkar, 2011 IEEE Biomedical Circuits and Systems Conference (BioCAS), 333-336 (2011).
[22] Y. Rondelez, Phys. Rev. Lett, **108**, 018102 (2012).
[23] M. Carbonell-Ballestero, E. Garcia-Ramallo, R. Montañez, C. Rodriguez-Caso, and J. Macía, Nucleic Acids Research, **44**(1), 496-507 (2016).
[24] N. A. Cookson, W. H. Mather, T. Danino, O. Mondragón-Palomino, R. J. Williams, L. S. Tsimring, and J. Hasty, Molecular Systems Biology, **7**, 561 (2011).
[25] H. d'A. Heck, J. Am. Chem. Soc. **93**, 23-29 (1971).
[26] S. B. Cahn and S. G. J. Mochrie, American Journal of Physics **82**, 412 (2014).
[27] P. Smolen, D. A. Baxter, and J. H. Byrne, American Journal of Physiology-Cell Physiology **274**, C531-C542 (1998).
[28] L. Giri, V. K. Mutalik, K. V. Venkatesh, Theoretical Biology and Medical Modelling **1**, 2 (2004).
[29] F. Wu, D. J. Menn, and X. Wang, Chemistry & Biology **21**, 1629-1638 (2014).
[30] J. H. J. Leveau and S. E. Lindow, Journal of Bacteriology **183**, 6752-6762 (2001).
[31] R. Schleif, FEMS Microbiol. Rev. **34**, 779-796 (2010).
[32] M. H. Zwietering, I. Jongenburger, F. M. Rombouts, and K. van't Riet, Applied and Environmental Microbiology **56**, 1875-1881 (1990).
[33] F. Widdel, Di dalam Grundpraktikum Mikrobiologie **4**, 1-11 (2007).
[34] S. Taheri-Araghi, S. Bradde, J. T. Sauls, N. S. Hill, P. A. Levin, J. Paulsson, M. Vergassola, and S. Jun, Current Biology **25**, 385-391 (2015).
[35] P. Wang, L. Robert, J. Pelletier, W. L. Dang, F. Taddei, A. Wright, and S. Jun, Current Biology **20**, 1099-1103 (2019).